Composites Part B 99 (2016) 305–311

Contents lists available at ScienceDirect

Composites Part B

journal homepage: www.elsevier.com/locate/compositesb

Surface roughness effects on the reinforcement of cement mortars through 3D printed metallic fibers

Ilenia Farina [a], Francesco Fabbrocino [b], Francesco Colangelo [a], Luciano Feo [c], Fernando Fraternali [c, *]

[a] Department of Engineering, University of Naples Parthenope, Centro Direzionale di Napoli, Isola C4, 80143, Naples, Italy
[b] Department of Engineering, Pegaso University, Piazza Trieste e Trento, 48, 80132, Naples, Italy
[c] Department of Civil Engineering, University of Salerno, Via Giovanni Paolo II 132, 84084, Fisciano, SA, Italy

ARTICLE INFO

Article history:
Received 27 February 2016
Received in revised form
9 April 2016
Accepted 23 May 2016
Available online 27 May 2016

Keywords:
Fibres
Fibre/matrix bond
Fracture toughness
Surface analysis
Additive manufacturing

ABSTRACT

We analyze the flexural reinforcement of a high-strength cement mortar using metallic fibers obtained via additive manufacturing of a powder of the titanium alloy Ti-6Al-4V. The analyzed fibers feature either macroscopic or microscopic surface roughness. Their surface morphology is characterized via optical and scanning electron microscopy. The results highlight that the flexural strength and fracture toughness of the examined mortar depend on the scale of the surface roughness of the reinforcing fibers. Specimens reinforced with fibers exhibiting microscopic surface roughness exhibit a pull through bonding mechanism between fiber and matrix, which causes limited matrix damage and a diffuse friction contribution to energy dissipation. Specimens reinforced with fibers exhibiting microscopic surface roughness, however, feature a pull through bonding mechanism that causes remarkable matrix damage. Comparisons with previous results relative to the reinforcement of a different cement mortar by the same fibers are established.

1. Introduction

Multiscale additive manufacturing (AM) technologies are advancing extremely quickly, for both the fabrication of materials and the diverse micro rapid prototyping of nozzles, micro filters, composite materials, and multiple integration for photonic circuits or microfluidic systems. The use of innovative materials in full-scale production is imminent, drawing on the continuous evolution of AM methods, the widening of material portfolios, and the progressive reduction of fabrication costs [1]. The use of AM technologies for the development of innovative composite materials is reviewed in Ref. [2], with special focus on carbon fiber reinforced thermoplastic composites. Nowadays, the most commonly employed AM techniques are the stereolithography (SLA) of liquid photopolymers, the fused deposition modeling (FDM) of plastic filaments, and the selective laser sintering (SLS) of metallic powders [1,2]. Effective composite filaments for FDM are produced by reinforcing thermoplastic materials with carbon fibers, glass fibers, and/or carbon nanotubes [2,3]. A matrix material for the rapid prototyping of electrically conductive elements was manufactured in Ref. [4], using a plaster-based powder, deposited layer-by-layer, and an inkjet printed liquid binder. Blends of thermoplastic starches (TPS), acrylonitrile-butadiene-styrene copolymers (ABS), compatibilizers, impact modifiers, and pigments were used in Ref. [5] for the manufacturing of eco-friendly FDM filaments featuring good mechanical properties, excellent workability and high thermal stability. The use of ultrasonic additive manufacturing (UAM) for creating metal-matrix composites is described in Refs. [6,7], which deal with the formulation and analysis of an innovative composite obtained by reinforcing an aluminum matrix with prestrained shape memory alloy fibers. These studies specifically investigate the strength of the fiber–matrix interface, which significantly characterizes the overall properties of UAM composites, through pullout tests, differential scanning calorimetry, and finite-element simulations.

A recent work has explored the use of additively manufactured reinforcing fibers of cement mortars [8] for use, e.g., in the structural retrofitting of existing buildings and historical constructions [9–11]. The reinforcing elements analyzed in Ref. [8] consist of fibers with a structural hierarchy manufactured from computer-

* Corresponding author.
E-mail address: f.fraternali@unisa.it (F. Fraternali).

http://dx.doi.org/10.1016/j.compositesb.2016.05.055
1359-8368/

aided design (CAD) data, employing additive manufacturing techniques based either on photopolymers (SLA) or the electron beam melting (EBM) of a powder of the titanium alloy Ti-6Al-4V [12–15]. EBM is a SLS technology that allows the manufacture of features with sizes as low as 0.4 mm by progressively depositing, heating and melting layers of metallic powders, with the melted regions in each layer defined according to a CAD model of the specimen to be manufactured [14,15]. The study presented in Ref. [8] is aimed at exploring the potential of AM technologies to replicate surface treatments of reinforcing bars such as, e.g., sand-coating [16] and carbon nanotube enrichment [17,18], for use in the optimal tensile strengthening of cementitious materials.

The present work expands upon existing research by examining the reinforcement of a high-strength cement mortar [9] using the same Ti-6Al-4V fibers studied in Ref. [8]. We begin in Sec. 2 by describing the preparation of the analyzed mortar and fibers. We then pass to an analysis of the results of short-beam shear tests aimed at determining the first-crack strength and toughness of the current fiber-reinforced mortar, while establishing comparisons with the results presented in Ref. [8] (Sec. 3). Next, we focus our attention on the microscopy characterization of the surface morphologies of the Ti-6Al-4 fibers (Sec. 4). By comparing the results of the present study with those available in Ref. [8], we are able to draw some conclusions about the influence of the surface roughness scale effects of the reinforcing fibers (microscopic or macroscopic roughness) on the mechanical response of high-strength and low-strength cement mortars. We end in Sec. 5 with concluding remarks and suggestions for future research.

2. Materials

We analyze the Disbocret Unitech R4 mortar produced by Italian Caparol GmbH & Co – a commercial mortar reinforced with PVC micrometric fibers (~50 μm diameter, ~1 mm length) used for repairing damaged concrete (see Table 1 for the producer datasheet giving mechanical properties). This mortar is reinforced with two different cylindrical fibers (or bars) made of the titanium alloy Ti-6Al-4V (hereafter, Ti6Al4V) [8], comprising both macroscopically smooth fibers with 7.5 mm diameter ("Ti_S" fibers, see Fig. 1 a,b), and macroscopically rough fibers with 7.0 mm diameter and coated with a 0.75 mm × 0.75 mm grid of cylindrical embossments. The latter exhibit 0.20 mm diameter and 0.50 mm length ("Ti_R" fibers, cf. Fig. 1 c,d).

The special nature of the reinforcing elements illustrated in Fig. 1 is explained by our future intention to examine the reinforcement of concretes with metallic bars obtained through AM technologies. Due to current limitations of the EBM technology in manufacturing objects with a maximum build size greater than 200 mm, we decided to employ these elements for the reinforcement of a cement mortar instead of a concrete with reduced scale aggregates.

The manufacturing process of the fibers/rebars in Fig. 1 starts with the progressive deposition, heating and melting of layers of a Ti4Al6V powder. A sliced version of the CAD model of the fibers is then processed via the EBM facility Arcam S12 [8]. The Ti4Al6V powder consists of spherical particles with 45–100 μm diameter. The raw material is ASTM Grade 5 (6al-4V) [12]. The melting phase is preceded by a preheating stage, during which the powder is sintered by rapidly scanning the beam (using standard Arcam parameters), in order to maintain the target build temperature of 730 °C. The subsequent melting stage makes use of the three-beam rastering strategies diffusely illustrated in Ref. [19], a beam current of 1.7 mA, and a beam speed of 200 mm/s. The voltage is kept constant at 60 kV. Once manufactured, all remnants of unmelted powder are removed using compressed air.

The above mentioned dimensions of the Ti6Al4V fibers refer to the CAD models, and do not correspond perfectly to the built object, since the beam scan strategies of the EBM process and the surface roughness generally result in larger (in diameter) printed members [10–12] (cf. Sec. 4). The main properties of the fully dense Ti6Al4V alloy are given in Table 1 [13]. Recent investigations on porosity in EBM titanium parts made with the same conditions used for the current material [12] have shown that the internal porosity is of the order of 0.2% or less. For this reason, we hereafter assume that the Young modulus of the porous material is approximately equal to that of the fully dense Ti6Al4V alloy [13,20].

Prismatic 40 mm × 40 mm × 160 mm specimens of the Disbocret Unitech R4 mortar were reinforced with Ti_S and Ti_R fibers, using a mortar cover of 7 mm (effective depth equal to 33 mm). The remainder of the paper makes use of the labels Ti_R, and Ti_S to denote the mortar specimens reinforced with the corresponding Ti6Al4V fibers, and the label UNR to denote unreinforced mortar specimens. We manufactured three Ti_R specimens, two Ti_S specimens, and two UNR specimens.

3. Short-beam shear tests

We studied the mechanical response of fiber-reinforced mortar specimens by carrying out short-beam shear (SBS) tests in displacements control with a 0.50 mm/min loading rate, after 28 days of curing. These tests consist of three-point bending tests performed on a clear length $L = 100$ mm of the mortar specimens described in Sec. 1 (Fig. 2).

The applied load (F) versus mid-span deflection (δ) curves obtained for the analyzed specimens under the SBS tests are shown in Fig. 3. Figs. 4 and 5 illustrate frames taken from in-situ videos of the SBS tests performed on the specimens Ti_S_1 and Ti_R_1, respectively. Finally, Fig. 6 provides pictures of the configurations after SBS testing of selected specimens.

3.1. First crack strength and fracture toughness

Following [8] (see also ASTM C1018 [21]), we characterize the fracture toughness of the fiber-reinforced mortar via the index:

Table 1
Mechanical properties of analyzed mortar and fibers.

Disbocret Unitech R4 mortar
Compressive strength ≥45 MPa (class R4 - EN 1504) Bond to existing concrete ≥ 2 MPa (EN 1542) Young's modulus ≥ 20 GPa (EN 13412)
Ti6Al4V titanium alloy
Mass density 4430 kg/m^3 Tensile strength 950 MPa Young's modulus 120 GPa

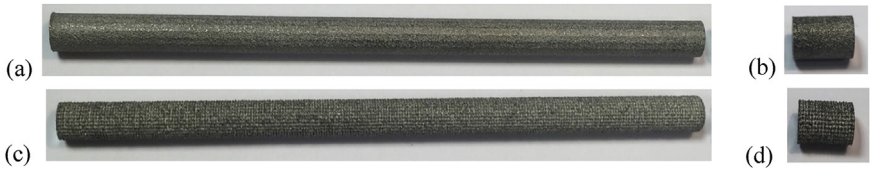

Fig. 1. Full size views and cut parts of Ti_S (a,b) and Ti_R (c,d) fibers.

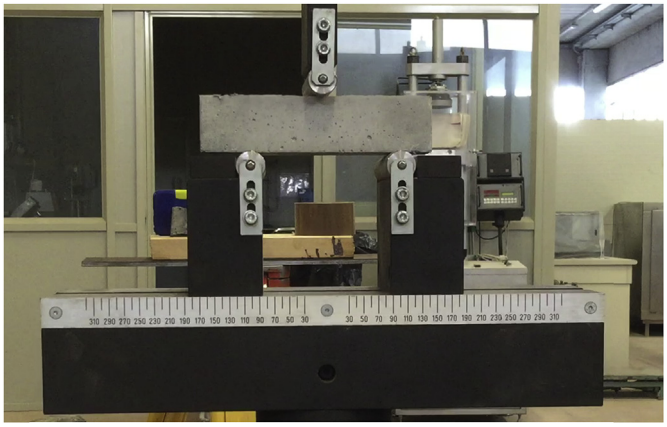

Fig. 2. Setup of short-beam shear tests.

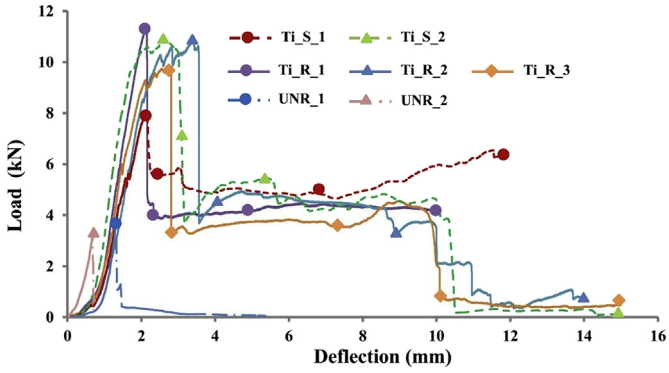

Fig. 3. Force vs. deflection curves of Ti_S, Ti_R and UNR specimens.

$$I = \frac{A\left(\delta = 3\bar{\delta}\right)}{A_{UNR}\left(\bar{\delta}\right)} \tag{1}$$

Here, $\bar{\delta}$ is the mid-span deflection at the first crack load; $A(\delta = 3\bar{\delta})$ is the area under the load-deflection curve from the origin up to $\delta = 3\bar{\delta}$; and $A_{UNR}(\bar{\delta})$ is the mean value of the area under the load-deflection curve of UNR specimens up to crack opening. We also investigate the first crack strength by computing the maximum tensile stress f_{cr} carried by the material in correspondence with the first crack load F_{cr}, assuming linear elastic behavior up to crack initiation, the material properties in Prismatic 40 mm × 40 mm × 160 mm specimens of the Disbocret Unitech R4 mortar were reinforced with Ti_S and Ti_R fibers, using a mortar cover of 7 mm (effective depth equal to 33 mm). The remainder of the paper makes use of the labels Ti_R, and Ti_S to denote the mortar specimens reinforced with the corresponding Ti6Al4V fibers, and the label UNR to denote unreinforced mortar specimens. We manufactured three Ti_R specimens, two Ti_S specimens, and two UNR specimens.

Table 1, and homogenized properties for the fiber-reinforced cross-section [22]. Table 2 gives the first crack strength f_{cr} and the toughness index I of the tested specimens, together with the mean values of these quantities for each examined material (denoted by $\bar{f}_{cr}$ and $\bar{I}$, respectively).

The results presented in Figs. 3–6 and Table 2 highlight the fact that the reinforcement of the examined mortar with Ti_R fibers greatly enhances the first-crack strength ($\bar{f}_{cr} = 19.45$ MPa) and fracture toughness ($\bar{I} = 39.40$), compared with the case of the unreinforced material (which exhibits $\bar{f}_{cr} = 8.67$ MPa and brittle response after crack onset, despite the presence of PVC micrometric fibers, cf. Fig. 3). Reinforcement with Ti_S fibers also produces remarkable increases in the above quantities compared with the UNR case ($\bar{f}_{cr} = 17.48$ MPa; $\bar{I} = 36.09$), even though the value of $\bar{f}_{cr}$ for Ti_S specimens is appreciably smaller than for Ti_R specimens. It is worth noting, however, that reinforcement with Ti_S fibers may lead to a residual load-carrying capacity of the fractured material (after crack onset), which is almost equal to or even slightly greater than that resulting from reinforcement with Ti_R fibers. This effect is clearly visible in Fig. 7, which shows a comparison between the load-deflection curves of specimens made from the mortar examined in the present study ("a" specimens) and the low-strength mortar examined in Ref. [8] ("b" specimens).

The results in Fig. 7 and Table 2 highlight the fact that the residual load-carrying capacity (after crack onset) and the toughness index I of the Ti_S_1a specimen are greater than the analogous quantities of the Ti_R1a specimen. On average, the toughness index of Ti_R_a specimens is only 9% greater than that of Ti_S_a specimens (cf. Table 2). This beneficial effect of Ti_S fibers is less pronounced in the case of "b" specimens (weak mortar). The $\bar{I}$ index of the Ti_S_b specimens is significantly (23%) smaller than that of the Ti_S_b specimens (cf. Table 2 of Ref. [8]). It can be argued that the macroscopic roughness of the Ti_R fibers may induce a pull-through bond failure mode, which increases the first-crack strength, but may partially compromise the energy absorption capacity of the material (cf. Sec. 4).

Concerning the failure mechanism under SBS tests, the images in Figs. 4–6 show a shear-type failure affected by diagonal cracks in the Ti_S and Ti_R specimens. UNR specimens, however, exhibit flexural-type failure due to the vertical (or sub-vertical) propagation of the central crack up to failure (cf. Fig. 6).

3.2. Shear capacity

Having denoted the fiber cross-sectional area by A_s and the effective depth of the cross section by d, we now compare the experimental results in Fig. 3 with the following predictions of the shear capacity of the examined materials, which are respectively provided by the international standards EC2 [22], ACI 318 [23] and BS 8110-1 [24].

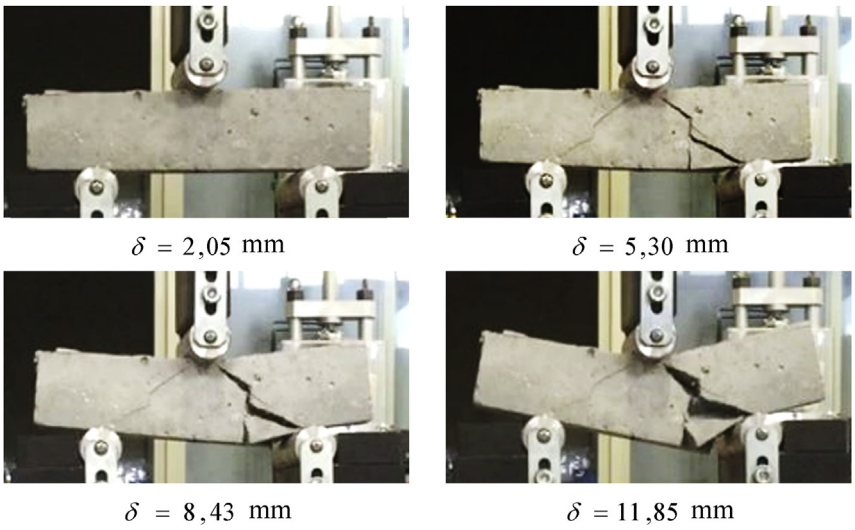

Fig. 4. Frames from an in-situ video of the SBS test on the Ti_S_1 specimen.

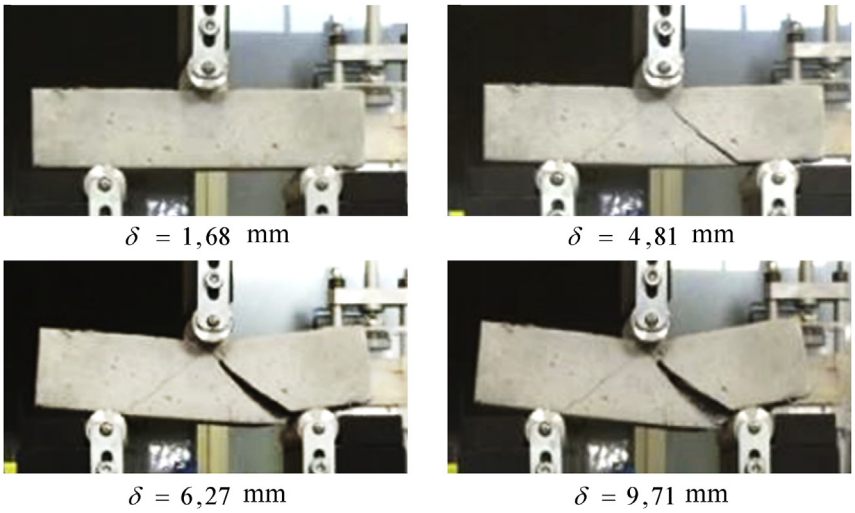

Fig. 5. Frames from an in-situ video of the SBS test on the Ti_R_1 specimen.

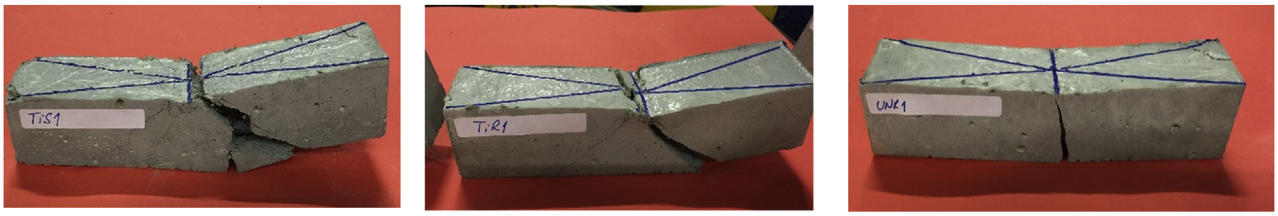

Fig. 6. Pictures of different specimens taken after the completion of SBS tests.

$$V_{Rd}^{EC2} = \min\left\{\frac{0.18}{\gamma_c}k\left(100\frac{A_s}{bd}f_{ck}\right)^{1/3},\ 0.035\left(1+\sqrt{\frac{200}{d}}\right)^{\frac{3}{2}}\sqrt{f_{ck}}\right\}bd \quad (2)$$

$$V_{Rd}^{ACI} = 0.17\phi_c\sqrt{f_{ck}}bd \quad (3)$$

$$V_{Rd}^{BS} = \frac{0.79}{\gamma_M}\left(100\frac{A_s}{bd}\right)^{\frac{1}{3}}\left(\frac{400}{d}\right)^{\frac{1}{4}}\left(\frac{f_{ck}}{25}\right)^{\frac{1}{3}}bd \quad (4)$$

Here f_{ck} denotes the characteristic compressive strength of the mortar ($f_{ck} = 45$ MPa, cf. Table 1); and we set: $\gamma_M = 1.25$, $\phi_c = 0.85$, $\gamma_c = 1.5$.

Table 3 compares the predictions of the shear capacities of the examined materials with the experimental capacities $\overline{V}_{\exp}$

Table 2
First crack strength f_{cr} and toughness index I of the materials examined in the present study.

Specimen	f_{cr} (MPa)	Mean value $\bar{f}_{cr}$ (MPa)	Specimen	I	Mean value $\bar{I}$
Ti_S_1	14.85	17.48	Ti_S_1	31.90	36.09
Ti_S_2	20.11		Ti_S_2	40.28	
Ti_R_1	21.12	19.45	Ti_R_1	30.31	39.40
Ti_R_2	19.15		Ti_R_2	52.75	
Ti_R_3	18.08		Ti_R_3	35.12	
UNR_1	9.16	8.67			
UNR_2	8.18				

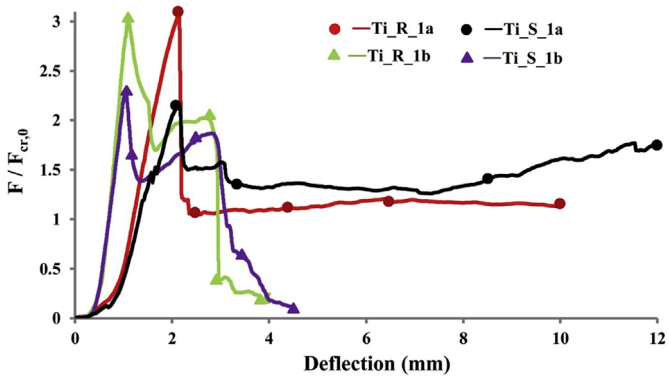

Fig. 7. Comparison of force vs. deflection curves of specimens made of the high-strength mortar analyzed in the present study ("a" specimens) and the low-strength mortar analyzed in Ref. [8] ("b" specimens). $F_{cr,0}$ denotes the first crack load of the unreinforced material.

Table 3
Comparison between experimental and theoretical predictions of the shear capacity of Ti_R and Ti_S specimens.

Specimen	d (mm)	A_s (mm^s)	$\overline{V}_{exp}$ (kN)	V_{Rd}^{BS} (kN)	V_{Rd}^{ACI} (kN)	V_{Rd}^{EC2} (kN)
Ti_R	33	38.48	4.71	2.39	1.28	2.00
Ti_S	33	38.48	5.24	2.39	1.28	2.00

corresponding to half of the peak loads observed in Fig. 3 (averaged among all specimens). This comparison reveals that all the examined standards significantly underestimate the shear capacities of the Ti_R and Ti_S specimens in the present work (as opposed to those observed in Ref. [8]), completely ignoring the role played by the surface microstructure of the reinforcing elements with respect to the shear response of the composite material.

4. Microscopy characterization of the fiber roughness

We first investigated the surface roughness of Ti_S and Ti_R fibers using the "crack width" optical microscope by Controls® to take images of the surface of the fibers with 40 × magnification (Fig. 8). The images in Fig. 8 show a clear difference in the roughness of the fibers. It is seen that the outer surface of Ti_S fibers features "microscopic" asperities (size: ~0.05 mm), which are characteristic of EBM manufactured parts [12–15]. Conversely, the outer surface of Ti_R fibers shows "macroscopic" asperities (~0.50 mm).

The surface morphology of Ti_S and Ti_R fibers was also characterized using the Phenom ProX Scanning Electron Microscopy (SEM) apparatus (Figs. 9 and 10). The SEM investigation targeted the interfacial transition zone (ITZ) between the cement paste and the fibers, as well as the ITZ for aggregates, as the morphology of such regions is of fundamental importance for the mechanical and physical properties of cement mortars [25–27]. SEM images were taken of 0.5 cm length parts cut from the 3D printed fibers (Fig. 1 b,d) using different magnification factors. The images in Fig. 9 confirm that the surface of the Ti_S fibers is not actually smooth, being affected by microscopic asperities and appreciable porosity. It is also worth noting that the smooth areas of Ti_S fibers (white regions in Fig. 9) do not hold mortar pieces after the fiber pullout, while mortar particles are attached to the depressed regions of the outer surface of the fibers.

The SEM characterization of the morphology of the Ti_R fibers reveals that the built size of the macroscopic embossments of these fibers does not correspond to the CAD size, as previously observed [13–15] (cf. Fig. 10). The macroscopic roughness of Ti_R fibers results in remarkable matrix damage after pullout, as confirmed by the presence of mortar particles attached to both valleys and crests of the pulled-out fibers (Fig. 10).

The results of the SBS tests presented in Sec. 3, and the morphologies of the Ti_S and Ti_R fibers after pullout, indicate that Ti_S specimens are affected by a weaker fiber matrix bond compared to Ti_R specimens. Nevertheless, Ti_S specimens exhibit a very effective pull-through bonding mechanism between fiber and matrix, which causes limited matrix damage and a diffuse friction contribution to energy dissipation (cf. Fig. 9) [28]. This is essentially due to the role played by the transverse pressure on the stress vs. slip response of the fiber-matrix interface [17]. Ti_R specimens instead feature a less effective pull through bonding mechanism that causes marked matrix damage (Fig. 10). The presence of large matrix debris between the protrusions of the Ti_R fibers indicates interfacial failure caused by the matrix crushing against the pullout [17].

5. Concluding remarks

We investigated the reinforcement of a high-strength cement mortar using 3D printed fibers made of the Ti6Al4V titanium alloy, which were additively manufactured via electron beam melting. Short-beam shear tests in displacements control have shown high enhancements in the first-crack strength and fracture toughness of the analyzed mortar, both in the presence of reinforcing fibers with microscopic roughness (Ti_S fibers), and in the case of reinforcing fibers with macroscopic roughness (Ti_R fibers).

Mortar reinforcement with Ti_R fibers proved to be the most effective in terms of first-crack strength enhancement over the unreinforced material. We also noticed that the reinforcement with Ti_S fibers led to a residual load-carrying capacity of the cracked mortar that is almost equal to or even slightly greater than that of the mortar reinforced with Ti_R fibers. This beneficial effect of Ti_S fibers was less pronounced in the case of the fiber reinforcement of low-strength cement mortar analyzed in Ref. [8] (cf. Sec. 3). SEM and optical microscope analyses of the morphology of Ti_S and Ti_R fibers after pullout from the matrix revealed a pull-through bond failure mode in all the fiber-reinforced mortar specimens studied here (Sec. 4). The bonding mechanisms between fiber and matrix caused limited matrix damage and a diffuse friction contribution to

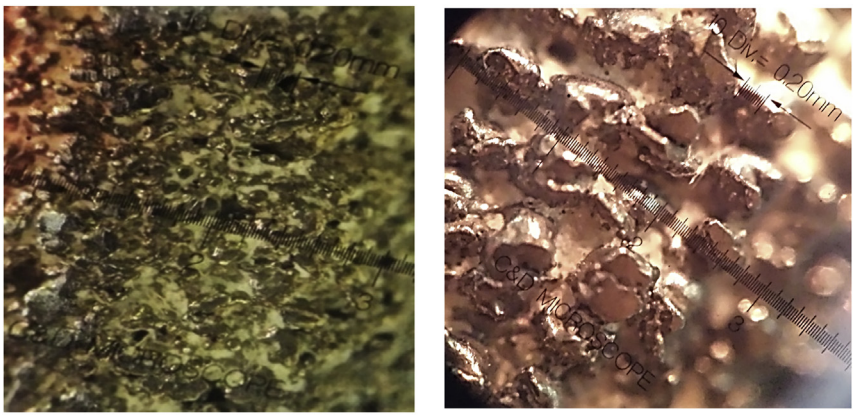

Fig. 8. Optical microscope images (40 × magnification) of Ti_S and Ti_R fibers.

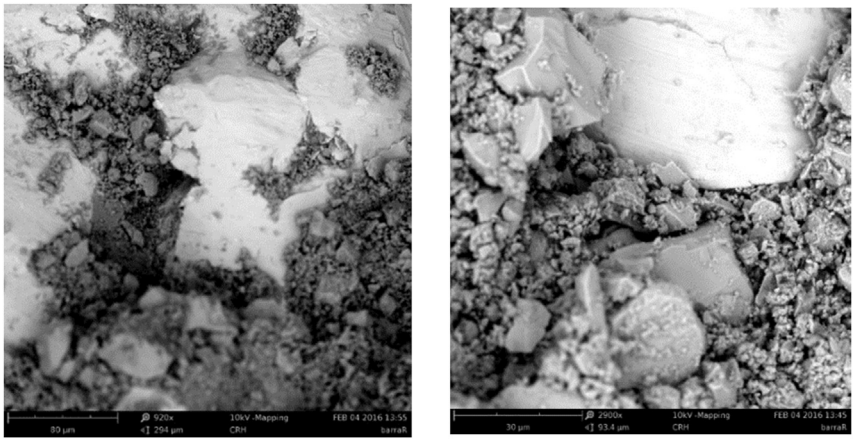

Fig. 9. SEM images with different magnifications of Ti_S fibers after pullout.

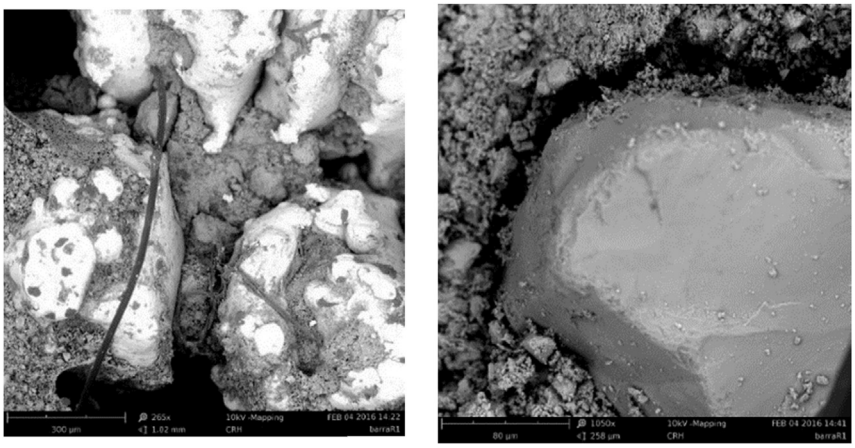

Fig. 10. SEM images with different magnifications of Ti_R fibers after pullout.

energy dissipation in the case of Ti_S fibers, and marked matrix damage in the case of Ti_R fibers.

The outcomes of the present study highlight that the morphology of the reinforcing fibers plays an important role in the energy absorption capacity and first-crack strength of cement mortars. We observed that an optimized design of the fiber surface

morphology may lead to increases or decreases in target mechanical parameters (such as, e.g, flexural strength and fracture toughness), depending on the nature of the matrix material.

The present study represents a first step towards studying concrete reinforcement with additively manufactured rebars in metallic materials, taking into account the different possible surface textures of these elements. The results presented in Secs. 3 and 4 prove that the international standards for the shear capacity of building materials not equipped with transverse shear reinforcements should be adequately generalized, in order to account for the actual nature and scale of the microstructure of longitudinal reinforcements.

It is worth noting that the reinforcement of composite materials through reinforcing fibers with nano-, micro- and macro-scale features can be investigated through an integrated approach that includes computational design and the additive manufacturing of physical models via innovative material deposition techniques [1–4,8]. With mechanical metamaterials' properties being dependent on the geometry of the microstructure, it makes no sense to carry out material development without design input; similarly, as material properties are dependent on processing conditions that remain poorly understood for many AM approaches, design in isolation from material understanding would not be effective.

In future work, we intend to carry out a micromechanics study into the bonding mechanisms between the fibers in the present study and cement mortars. Additional directions for future research include the computational modeling of the fiber-matrix bond mechanism [29,30], and engineering applications of innovative, fiber-reinforced mortars for the structural strengthening of existing constructions [10,11].

Acknowledgements

The authors are grateful to Ada Amendola and Gerardo Carpentieri (Department of Civil Engineering, University of Salerno, Italy), and Christopher Smith and Russell Goodall (Department of Materials Science and Engineering, University of Sheffield, UK) for their precious assistance with the manufacturing of the Ti-6Al-4V fibers and their help with the numerical post-processing of experimental results. The authors also wish to thank the Geoconsult Laboratory of Manocalzati (Avellino) for technical support provided during the SBS tests.

References

[1] Wohlers T. Wohlers report 2015: 3D printing and additive manufacturing state of the industry. Annual Worldwide Progress Report. Fort Collins, CO: Wohlers Associates, Inc.; 2015. ISBN 978-0-9913332-1-9.
[2] Ning F, Cong W, Qiu J, Wei J, Wang S. Additive manufacturing of carbon fiber reinforced thermoplastic composites using fused deposition modeling. Compos Part B Eng. 2015;80:369–78.
[3] Tekinalp HL, Kunc V, Velez-Garcia GM, Duty CE, Love LJ, Naskar AK, et al. Highly oriented carbon fiber-polymer composites via additive manufacturing. Compos Sci Technol 2014;105:144–50.
[4] Czyzewski J, Burzyński P, Gaweł K, Meisner J. Rapid prototyping of electrically conductive components using 3D printing technology. J Mater Process Tech 2009;12–13:5281–5.
[5] Kuo CC, Liu LC, Teng WF, Chang HY, Chien FM, Liao SJ, et al. Preparation of starch/acrylonitrile-butadiene-styrene copolymers (ABS) biomass alloys and their feasible evaluation for 3D printing applications. Compos Part B Eng 2016;86:36–9.
[6] Hahnlen R, Dapino MJ. NiTi-Al Interface strength in ultrasonic additive manufacturing composites. Compos Part B Eng 2014;59:101–8.
[7] Hehr A, Dapino MJ. Interfacial shear strength estimates of NiTi-Al matrix composites fabricated via ultrasonic additive manufacturing. Compos Part B Eng 2015;77:199–208.
[8] Farina I, Fabbrocino F, Carpentieri G, Modano M, Amendola A, Goodall R, et al. On the reinforcement of cement mortars through 3D printed polymeric and metallic fibers. Compos Part B Eng 2016;90:76–85.
[9] Fraternali F, Farina I, Polzone C, Pagliuca E, Feo L. On the use of R-PET strips for the reinforcement of cement mortars. Compos Part B Eng 2013;46:207–10.
[10] Fraternali F, Carpentieri G, Modano M, Fabbrocino F, Skelton RE. A tensegrity approach to the optimal reinforcement of masonry domes and vaults through fiber-reinforced composite materials. Compos Struct 2015;134:247–54.
[11] Fabbrocino F, Farina I, Berardi VP, Ferreira AJM, Fraternali F. On the thrust surface of unreinforced and FRP-/FRCM-reinforced masonry domes. Compos Part B Eng 2015;83:297–305.
[12] Amendola A, Nava EH, Goodall R, Todd I, Skelton RE, Fraternali F. On the additive manufacturing and testing of tensegrity structures. Compos Struct 2015;131:66–71.
[13] Amendola A, Smith CJ, Goodall R, Auricchio F, Feo L, Benzoni G, et al. Experimental response of additively manufactured metallic pentamode materials confined between stiffening plates. Compos Struct 2016. http://dx.doi.org/10.1016/j.compstruct.2016.01.09. Online First.
[14] Hernandez-Nava E, Smith CJ, Derguti F, Tammas-Williams S, Leonard F, Withers PJ, et al. The effect of density and feature size on mechanical properties of isostructural metallic foams produced by additive manufacturing. Acta Mater. 2015;85:387–95.
[15] Smith CJ, Derguti F, Hernandez-Nava E, Thomas M, Tammas-Williams S, Gulizia S, et al. Dimensional accuracy of Electron Beam Melting (EBM) additive manufacture with regard to weight optimized truss structures. J Mater Process Tech 2016;229:128–38.
[16] Kim B, Doh JH, Yi CK, Lee JY. Effects of structural fibers on bonding mechanism changes in interface between GFRP bar and concrete. Compos Part B Eng 2013;45(1):768–79.
[17] Donnini J, Corinaldesi V, Nanni A. Mechanical properties of FRCM using carbon fabrics with different coating treatments. Compos Part B Eng 2016;88:220–8.
[18] Jia Y, Chen Z, Yan W. A numerical study on carbon nanotube pullout to understand its bridging effect in carbon nanotube reinforced composites. Compos Part B Eng 2015;81:64–71.
[19] Tammas-Williams S, Zhao H, Léonard F, Derguti F, Todd I, Prangnell PB. XCT analysis of the influence of melt strategies on defect population in Ti–6Al–4V components manufactured by selective electron beam melting. Mater Charact 2015;102:47–61.
[20] Handbook Metals. (2) Properties and selection: nonferrous alloys and special-purpose materials. Metals Park, OH: ASM International; 1990.
[21] ASTM C1018 American Society for Testing and Materials. Standard test method for flexural strength of fiber reinforced concrete. Book of ASTM Standards. Barr Harbor Drive (West Conshohocken, PA, United States): ASTM; 1998.
[22] EN 1992-1-1. Eurocode 2. In: Design of concrete structures – Part 1-1: general rules and rules for buildings; 2004.
[23] ACI Task Committee 318. Building code requirements for structural concrete (ACI 318-08) and commentary. Farmington Hills: American Concrete Institute; 2008.
[24] BS8110-1. Structural use of concrete, part 1: code of practice for design and construction. London: British Standards Institute; 1997.
[25] Colangelo F, Messina F, Cioffi R. Recycling of MSWI fly ash by means of cementitious double step cold bonding pelletization: technological assessment for the production of lightweight artificial aggregates. J Hazard Mater 2015;299:181–91.
[26] Iucolano F, Liguori B, Caputo D, Colangelo F, Cioffi R. Recycled plastic aggregate in mortars composition: effect on physical and mechanical properties. Mater Des 2013;52:916–22.
[27] Cioffi R, Colangelo F, Montagnaro F, Santoro L. Manufacture of artificial aggregate using MSWI bottom ash. Waste Manage 2011;31(2):281–8.
[28] Wetherhold RC, Corjon M, Das PK. Multiscale considerations for interface engineering to improve fracture toughness of ductile fiber/thermoset matrix composites. Compos Sci Technol 2007;67(11):2428–37.
[29] Fraternali F. Free discontinuity finite element models in two-dimensions for in-plane crack problems. Theor Appl Fract Mech 2007;47:274–82.
[30] Schmidt B, Fraternali F, Ortiz M. Eigenfracture: an eigen deformation approach to variational fracture. Multiscale Model Sim 2009;7(3):1237–66.